Journal of Biomedical Optics

BiomedicalOptics.SPIEDigitalLibrary.org

Axial resolution and signal-to-noise ratio in deep-tissue imaging with 1.7-μm high-resolution optical coherence tomography with an ultrabroadband laser source

Hiroyuki Kawagoe
Masahito Yamanaka
Norihiko Nishizawa

Hiroyuki Kawagoe, Masahito Yamanaka, Norihiko Nishizawa, "Axial resolution and signal-to-noise ratio in deep-tissue imaging with 1.7-μm high-resolution optical coherence tomography with an ultrabroadband laser source," *J. Biomed. Opt.* **22**(8), 085002 (2017), doi: 10.1117/1.JBO.22.8.085002.

Axial resolution and signal-to-noise ratio in deep-tissue imaging with 1.7-μm high-resolution optical coherence tomography with an ultrabroadband laser source

Hiroyuki Kawagoe,[a,*] Masahito Yamanaka,[b] and Norihiko Nishizawa[b]
[a]Nagoya University, Department of Quantum Engineering, Furo-cho, Chikusa-ku, Nagoya, Aichi, Japan
[b]Nagoya University, Department of Electronics, Furo-cho, Chikusa-ku, Nagoya, Aichi, Japan

Abstract. We investigated the axial resolution and signal-to-noise ratio (SNR) characteristics in deep-tissue imaging by 1.7-μm optical coherence tomography (OCT) with the axial resolution of 4.3 μm in tissue. Because 1.7-μm OCT requires a light source with a spectral width of more than 300 nm full-width at half maximum to achieve such high resolution, the axial resolution in the tissue might be degraded by spectral distortion and chromatic dispersion mismatching between the sample and reference arms. In addition, degradation of the axial resolution would also lead to reduced SNR. Here, we quantitatively evaluated the degradation of the axial resolution and the resulting decrease in SNR by measuring interference signals through a lipid mixture serving as a turbid tissue phantom with large scattering and absorption coefficients. Although the axial resolution was reduced by a factor of ~6 after passing through a 2-mm-thick tissue phantom, our result clearly showed that compensation of the dispersion mismatching allowed us to achieve an axial resolution of 4.3 μm in tissue and improve the SNR by ~5 dB compared with the case where dispersion mismatching was not compensated. This improvement was also confirmed in the observation of a hamster's cheek pouch in a buffer solution. [DOI: 10.1117/1.JBO.22.8.085002]

Keywords: optical coherence tomography; 1.7-μm wavelength window; deep-tissue imaging; axial resolution.

Paper 170279R received May 6, 2017; accepted for publication Jul. 14, 2017; published online Aug. 4, 2017.

1 Introduction

Optical coherence tomography (OCT) provides high-resolution cross-sectional images of biological tissues without the need for pretreatments, such as staining and sectioning.[1,2] Recent developments in light sources with ultrabroad spectral widths have resulted in significant improvements in the axial resolution of OCT, down to submicron levels.[3–7] Because of its high-resolution and noninvasive imaging capabilities, OCT has been widely used in clinical and biological research fields, including ophthalmology, dermatology, and neuroscience.[7–10]

For deep-tissue imaging with OCT, the 1.3-μm wavelength window has been generally used due to the smaller scattering coefficient compared with the 0.8- to 1.0-μm wavelength regions.[11,12] Despite relatively higher water absorption, recently, it was reported that the 1.7-μm wavelength window has the potential to enhance the penetration depth in the observation of turbid scattering tissue because of the lower signal attenuation in the tissue, which is determined mainly by multiple light scattering and water absorption.[13–17] Although the signal loss caused by water absorption increases in the longer-wavelength region, a local minimum of water absorption exists at 1.5 to 1.85 μm. Since the scattering coefficient becomes smaller as the wavelength becomes longer, the total signal attenuation at 1.7 μm in turbid scattering tissue is smaller than that at 1.3 μm.[13–17] So far, several groups, including us, have successfully demonstrated that 1.7-μm OCT provides enhanced penetration depth in the observation of opaque samples, such as lipid mixture, human skin, and mouse brain.[16–23] In Ref. 17, it was demonstrated that 1.7-μm OCT systems provide the penetration depth of more than 2 mm in observations of human fingertips, while the penetration depth of 1.3-μm OCT was restricted to less than 2 mm owing to a larger scattering coefficient at the wavelength. In the imaging of mouse brain tissues with 1.7-μm OCT systems, the penetration depth beyond 1.5 mm was realized.[21,23]

Recently, we developed OCT and optical coherence microscopy (OCM) in the 1.7-μm wavelength window using an ultrabroad supercontinuum (SC) fiber laser source with a wavelength band of 1.4 to 2.0 μm and realized an axial resolution of less than 4 μm in tissue, assuming a refractive index of 1.38.[18–21] However, because such a broad spectral bandwidth is required to realize high axial resolution in 1.7-μm OCT [in our case, 200 to 300 nm at full-width at half maximum (FWHM)] and there are strong water absorption peaks at 1.45- and 1.9-μm wavelengths, it is considered that the axial resolution would be worse in the observation of deeper tissue structures, where the spectral shape might be distorted by water absorption and light scattering and large chromatic dispersion might be produced by the tissue. If the chromatic dispersion becomes large, the OCT signal sensitivity, i.e., the signal-to-noise ratio (SNR), would also be reduced. So far, there have been some reports about degradation of the axial resolution in the observation of human eye structures with 0.8- to 1.3-μm OCT, which

*Address all correspondence to: Hiroyuki Kawagoe, E-mail: kawagoe.hiroyuki@e.mbox.nagoya-u.ac.jp

1083-3668/2017/$25.00 © 2017 SPIE

offers the axial resolution of around a few or submicron micrometers.[24–28] In those reports, it was revealed that the axial resolution is mainly degraded by water absorption and chromatic dispersion in the eyes, and it is possible to cancel out the degradation if the spectral distortion by water absorption is not so severe.[26–28] However, since eyes are low-scattering samples, we should presumably take into account light scattering when it comes to highly scattering samples, such as skin and brain. In particular, in the 1.7-μm OCT with a high axial resolution, the spectral shape may be affected more than in the case of 0.8- to 1.3-μm OCT due to the requirement for a broader spectral width. Although the previous studies have already demonstrated that the use of the 1.7-μm spectral band allows us to improve the penetration depth,[16–23] it still remains unclear whether 1.7-μm OCT imaging of deeper parts in turbid scattering tissues with high axial resolution is feasible or not.

In this paper, we experimentally investigated the impact of light scattering, water absorption, and chromatic dispersion on the axial resolution and SNR in deep-tissue imaging with 1.7-μm OCT using the SC fiber laser source with the spectral bandwidth of ~300 nm (FWHM) in the wavelength region. In this study, we observed mixtures of lipid, distilled water (H_2O), and heavy water (D_2O) with different lipid concentrations, which are often used as standard biological phantoms for evaluating the performance of optical imaging techniques, such as OCT and optical microscopy,[16,17,29,30] and we quantitatively evaluated the degradation of the axial resolution and the decrease of SNR caused by the mixtures. The results indicated that, although spectral distortion was caused in the mixture, the FWHM of the spectral shape of the OCT signals was almost unchanged, and it was possible to achieve an axial resolution of ~4.3 μm in tissue just by compensating for the chromatic dispersion mismatching even after passing through a 2-mm-thick layer of a mixture with a 10% lipid concentration. In addition, we also confirmed that the dispersion compensation improved not only the axial resolution but also the SNR. Our study clearly showed that it is feasible to realize 1.7-μm OCT imaging of deep sites in turbid scattering tissues with high axial resolution just by applying chromatic dispersion compensation.

2 Material and Methods

2.1 *1.7-μm High-Resolution Optical Coherence Tomography System*

Figure 1 shows a schematic diagram of the 1.7-μm time-domain OCT (TD-OCT) system with a custom-built broadband SC source, which was basically the same as that in Ref. 18. We confirmed that the measurement accuracy of axial resolution with our TD-OCT system was ± 0.12 μm through 30 times measurements of a point spread function of our OCT system, which was recorded by observing reflection light from a mirror surface placed at the focusing position in the sample arm. The SC source that we used, which is based on an ultrashort-pulse fiber laser and optical fibers, has a spectral width of ~300 nm (FWHM) at the center wavelength of 1.7 μm.[18] The SC light beam was divided into sample and reference beams through a Michelson interferometer composed of three fiber couplers. Depth scanning was performed by scanning a corner cube prism mounted on a galvanometer in the reference arm. The beam from the fiber coupler-based interferometer was collimated by an aspheric lens. The diameter of the collimated beam was ~3 mm. The

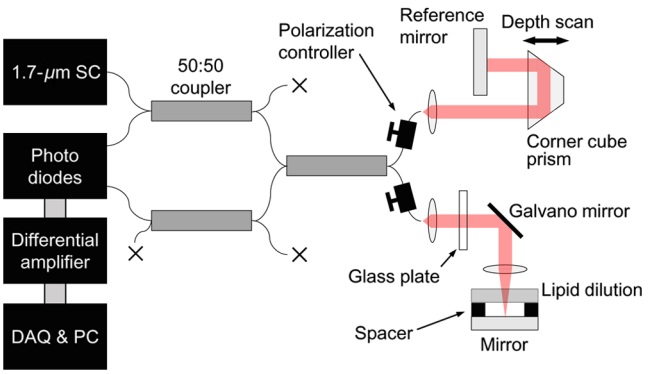

Fig. 1 Schematic diagram of the 1.7-μm TD-OCT system.

collimated beam was delivered to a scanning system with a telecentric design consisting of an X-galvanometer scanner and a focusing achromatic lens with a focal length of 30 mm (AC127-030-C-ML, Thorlabs). The backscattered and reflected light from both arms were made to interfere in the interferometer, and the interference signal was detected by a balanced detection system consisting of two extended-InGaAs photodetectors (PDA10D-EC, Thorlabs) and a differential amplifier circuit (5307, NF Corporation). The obtained interference signal was transferred to a personal computer equipped with a digitizer (PCI-5122, National Instruments) and was digitally bandpass-filtered to remove the DC component. The OCT signals were acquired using the squared detection method and were displayed on a logarithmic scale.[7] Before we measured the samples, the dispersion and polarization mismatches between the sample and reference arms were compensated for using optical glass plates (8-mm-thick fused silica) placed in the sample arm and polarization controllers. Based on the measurement result of dispersion mismatching between the sample and reference arms, the thickness of fused silica was chosen to minimize the dispersion mismatching.

2.2 *Spectral Analysis of Interference Signals*

To reveal the effects of water absorption, light scattering, and chromatic dispersion mismatching, we analyzed the optical spectrum and phase of the interference signals using Fourier transform analysis.[31] This spectral analysis method has been widely used to observe the light absorption and group delay of ultrafast pulses in optical materials and thin films.[32,33] The signal processing used in this work is briefly shown in Fig. 2. After measuring the interference signal [Fig. 2(a)], we applied a fast Fourier transform (FFT) with a Hanning window to the recorded interference signal to obtain the optical spectrum and phase of the interference signal [Fig. 2(b)]. To confirm the dispersion mismatch on the interference signal, we first fitted a fifth-order polynomial to the phase curve [Fig. 2(b)], and the fitted curve was differentiated [Fig. 2(c)]. Then, the second-order dispersion curve was obtained by differentiating the first-order derivative curve [Fig. 2(d)]. If the second-order dispersion becomes zero, we can obtain the highest axial resolution under the spectral width and shape, as shown in Fig. 2(b).[7] Note that the sign of the slope of the phase curve as a function of the wavelength in Fig. 2(b) is not important here because it changes depending on the position of the interference signal in a region where the FFT calculation is applied.

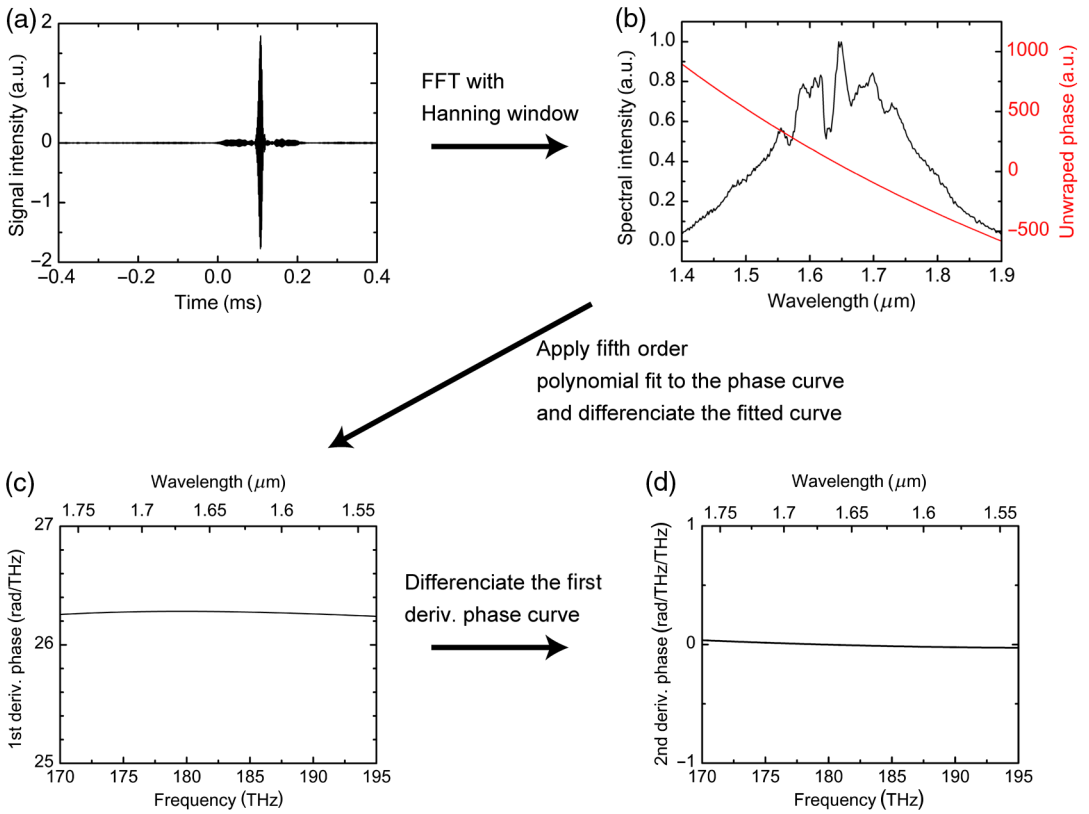

Fig. 2 Processing flow for investigating spectral distortion and dispersion: (a) recorded interference signal, (b) optical spectrum and phase, (c) first derivative of phase, and (d) second derivative of phase.

In this analysis, the spectral narrowing induced by scattering and absorption effects in the samples was evaluated by comparing the optical spectra of interference signals obtained from a mirror at the focus position with and without inserting the lipid mixture between the achromatic lens and mirror. The chromatic dispersion was confirmed from the second-order dispersion curve in Fig. 2(d). Here, we also calculated the achievable highest axial resolution by numerically compensating for the chromatic dispersion mismatching with a Fourier transform-based method.[26]

2.3 *Preparation of Biological Tissue Phantom*

For our study, we used mixtures of lipid, H_2O, and D_2O as biological tissue phantoms with large scattering and absorption coefficients. This kind of sample has been widely used as a tissue phantom for optical measurements.[16,17,29,30] According to a previous study,[16] the scattering coefficients of the mixture of 10 volume/volume % (v/v %) lipid, 70 v/v % H_2O, and 20 v/v % D_2O is ~3/mm in the 1.6-μm wavelength, which is similar to those of mouse brain.[34] Since skin and brain tissues have various scattering coefficients, we prepared mixtures with different lipid concentrations. For the lipid concentrations of 2, 5, and 10 v/v %, we diluted a lipid solution [lipid in H_2O (20 v/v %), Intralipos 20%, Otsuka Pharmaceutical Factory] with both H_2O and D_2O. A mixture without lipid (lipid concentration of 0 v/v %) was also prepared by mixing H_2O and D_2O. For all mixtures, the amount of D_2O in the mixtures was adjusted to set the H_2O concentration to 70 v/v %, which is similar to skin and brain tissues.[35,36] For example, when we prepared the mixture with the lipid concentration of 10%, we diluted 10 ml of the lipid solution (20 v/v %) with 4 ml of D_2O and 6 ml of H_2O. It is expected that the mixture of H_2O and D_2O (0 v/v % lipid concentration) will show almost the same absorption spectrum as H_2O because the absorption coefficient of D_2O is much smaller than that of H_2O in the wavelength range 1.4 to 2.0 μm.[37] We experimentally confirmed that the absorption coefficients of H_2O and D_2O are 0.54/mm and 0.036/mm at 1.7-μm wavelength, respectively. The mixture of H_2O and D_2O (70 v/v % H_2O, 30 v/v % D_2O, and 0 v/v % lipid concentration) had a similar absorption coefficient to 70 v/v % H_2O estimated by multiplying the absorption

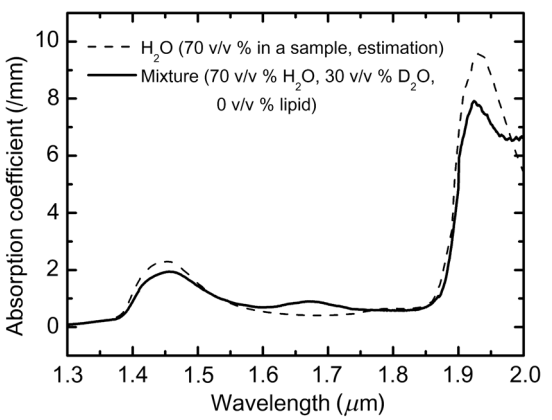

Fig. 3 Absorption coefficients of H_2O (dashed) and the mixtures of H_2O and D_2O (solid, 70 v/v % H_2O, 30 v/v % D_2O, and 0 v/v % lipid). The absorption coefficients of the mixtures were measured by a spectrophotometer (V-570, JASCO). The absorption coefficient of H_2O was obtained from Ref. 38 and was multiplied by 0.7 for comparison.

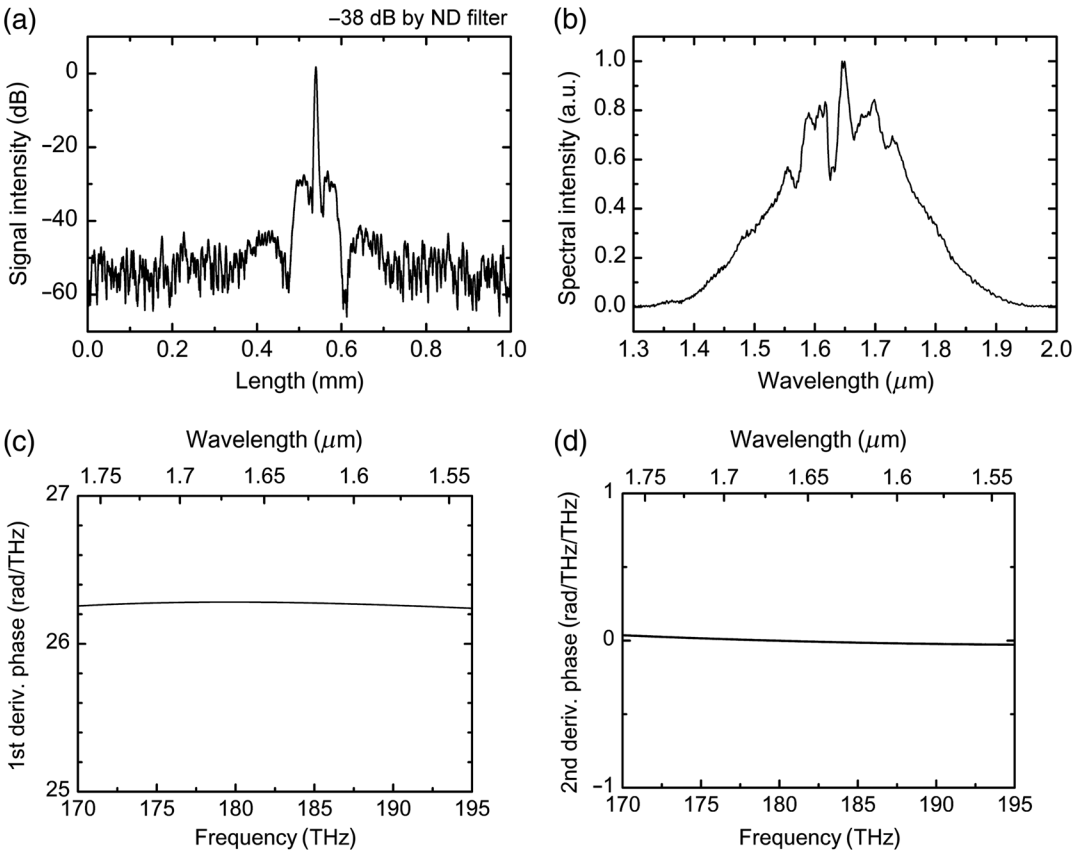

Fig. 4 (a) OCT signal obtained without any mixture, (b) the calculated optical spectrum, (c) first and (d) second derivative of the phase curve.

coefficient of H_2O in Ref. 38 by 0.7 (Fig. 3). The small absorption peak at 1.68 μm is presumably due to the absorption of semi-heavy water (HDO), which is formed only by mixing H_2O and D_2O.[39] The chromatic dispersion induced by D_2O can be ignored because it is quite small compared with that induced by H_2O.[40]

Although lipid has an absorption peak at 1.7 μm,[22,41] the absorbance of lipid is much smaller than that of H_2O, and the lipid concentration in the mixtures of lipid, H_2O, and D_2O is only 2 to 10 volume %. Therefore, we did not consider the absorption peak of lipid in our analysis.

To perform the measurement of OCT signals through the mixtures and evaluate the effects on the axial resolution and SNR, we filled quartz cuvettes with the mixtures and placed them above a sample mirror located at the focus position in the sample arm, as shown in Fig. 1. Since the penetration depth in 1.7-μm OCT imaging is typically 1 to 2 mm, we used quartz cuvettes with 1- and 2-mm path lengths.

3 Results

3.1 *Optical Coherence Tomography Signals Obtained without and with the Mixtures of Lipid, Distilled Water, and Heavy Water*

Figure 4(a) shows the OCT signal measured without any mixture placed in the sample arm. The axial resolution in tissue and the SNR were 3.6 μm and 93 dB, respectively. To avoid saturation of the detectors, we inserted a neutral density (ND) filter in the sample arm. The optical spectrum, the derivative of the phase of the interference signal, and the second-order dispersion are shown in Figs. 4(b)–4(d), respectively. From this result, although the shoulders near the main peak in Fig. 4(a) exist due to the spectral shape, we confirmed that the inherent dispersion mismatch in the interferometer was almost completely compensated for at all wavelengths in the optical spectrum of our 1.7-μm SC.

Figures 5(a) and 5(b) show the OCT signals obtained with 1- and 2-mm-thick mixtures (lipid concentrations are 0, 2, 5, and 10 v/v %), respectively. Compared with Fig. 4(a), the OCT signals were obviously blurred by passing through the mixtures. For the mixtures with greater thickness, the width of the OCT signals increased, as shown in Fig. 5(b). From the results of OCT signals with different thicknesses, we plotted the axial resolution and attenuation of SNR as a function of the lipid concentration [Figs. 5(c) and 5(d)]. For the 1- and 2-mm-thick mixtures, the axial resolution in the tissue increased to ~12.0 and ~21.9 μm, respectively. Compared with the axial resolution of 3.6 μm in the case of OCT imaging without any mixture, the resolution was increased by factors of 3.3 and 6.1 for the 1- and 2-mm-thick mixtures, respectively. Note that it is more likely that the axial resolution depended only on the thickness of the mixtures and not on the lipid concentration. It was also confirmed that multiple scattering in samples is not a main factor of degradation of the axial resolution by observing interference signals from the top and bottom sides of a glass cuvette filled with the 500-μm mixtures (lipid concentration: 0 v/v % and 10 v/v %). As shown in Fig. 6, the interference signals from the bottom surface of the cuvette were broadened by the mixtures. However, comparing the widths (at 6 dB down) of the

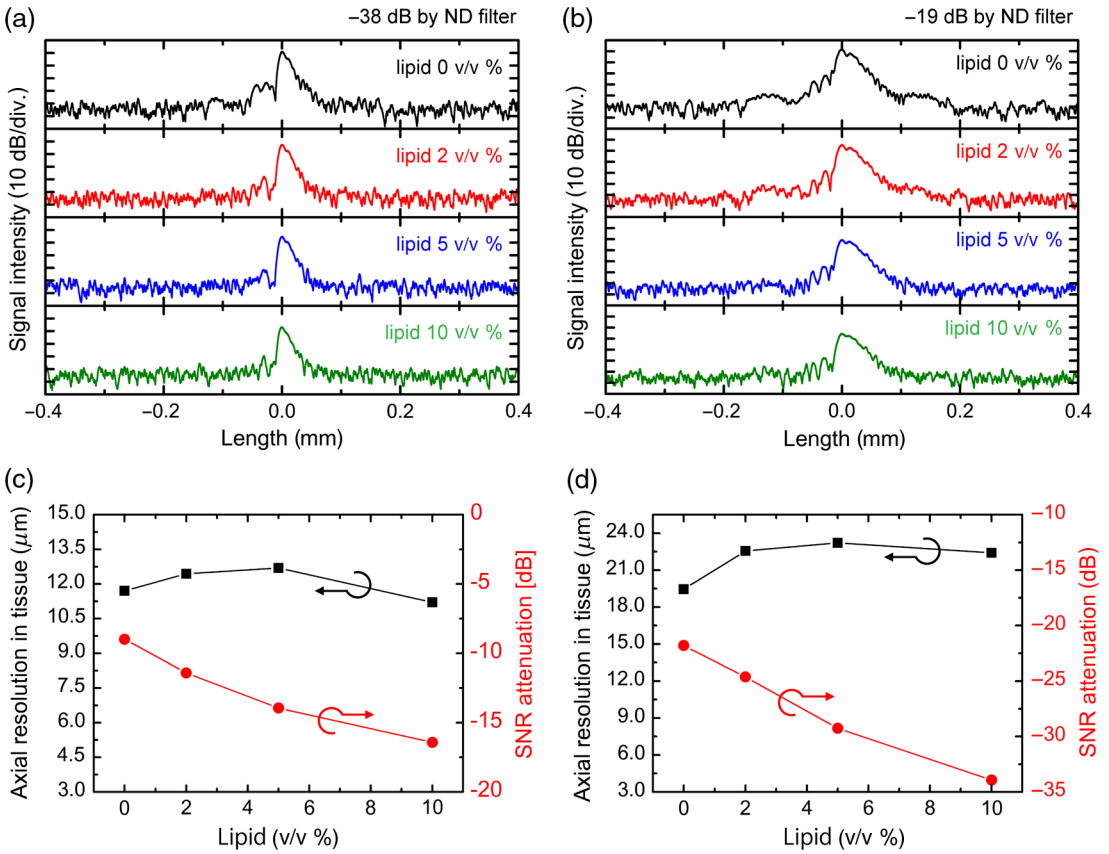

Fig. 5 OCT signals obtained with (a) 1- and (b) 2-mm-thick mixtures. Black, red, blue, and green lines correspond to the lipid concentrations of 0, 2, 5, and 10 v/v %, respectively. The axial resolution and SNR attenuation caused by passing through the (c) 1- and (d) 2-mm-thick mixtures are summarized as a function of the lipid concentration.

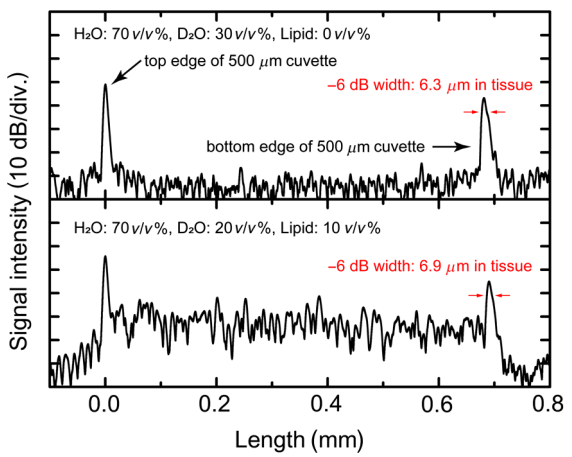

Fig. 6 OCT signals obtained with a 500-μm-thick cuvette filled with the mixture of 0 v/v % lipid dilution (upper) and 10 v/v % lipid dilution (lower).

interference signals in the case of 10 v/v % lipid with that in 0 v/v % lipid, there was only a small difference. Unlike in our case, previous reports using OCT in a shorter-wavelength region, such as 0.8 μm, indicated that multiple scattering in samples is also one of the main factors to degrade the axial resolution.[42] This difference is presumably attributed to the scattering coefficient (~3/mm) in the 1.7-μm region being smaller than those of the shorter wavelengths previously used for OCT measurements (e.g., 20/mm in 0.8-μm region).[42] On the other hand, the SNR monotonically decreased with increasing lipid concentration because of the associated increase in scattering coefficient.

3.2 *Spectral Distortion and Chromatic Dispersion Effects Induced by the Mixtures*

To reveal how much the water absorption and light scattering effects distort the optical spectra of the interference signals, we observed the optical spectra of the interference signals obtained with the mixtures [Figs. 7(a) and 7(b)]. The optical spectra were obtained by taking the FFT of the interference signals. With the mixtures, the spectral intensity at 1.45- and 1.9-μm wavelengths was significantly decreased due to the strong water absorption peaks at those wavelengths. The large spectral attenuation at 1.45 μm slightly shifted the peak position of the spectra to the longer-wavelength region. We also noticed that the attenuation of the spectral intensity in the shorter-wavelength region increased with increasing lipid concentration. This is due to the larger scattering coefficient at shorter wavelengths compared with that at longer wavelengths.[16,17,19] Thus, the redshift of the spectra was more obvious for the higher lipid concentrations. The center wavelength and FWHM of the spectra are summarized in Table 1. We found that the spectral widths (FWHM) of the spectra were slightly broadened after passing through the mixtures

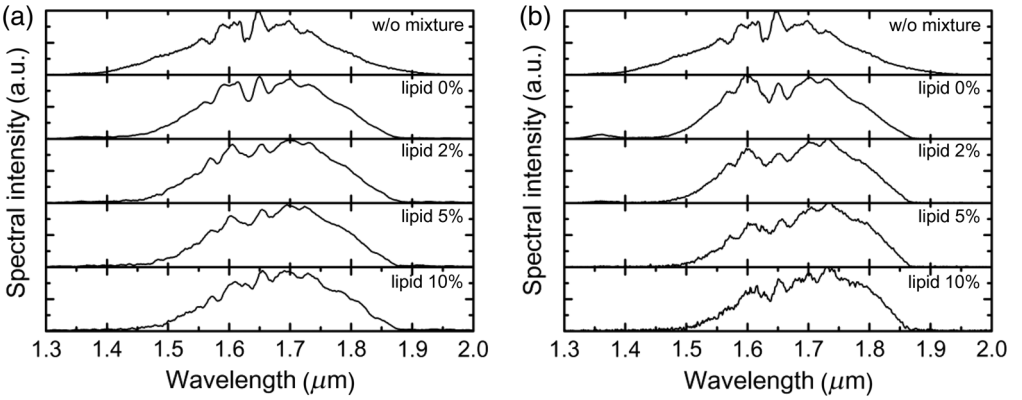

Fig. 7 Normalized optical spectra obtained by FFT of the interference signals for (a) 1- and (b) 2-mm-thick mixtures.

Table 1 Summary of the center wavelength and FHWM spectral width of the optical spectra. The achievable axial resolution calculated from the power spectra is also shown.

Liquid	Center wavelength (μm)	Spectral width (FWHM) (nm)	Achievable resolution in tissue (μm)
Without mixtures	1.65	210	3.3
Lipid 0% 1 mm	1.67	238	3.7
Lipid 2% 1 mm	1.68	244	3.8
Lipid 5% 1 mm	1.68	246	3.9
Lipid 10% 1 mm	1.69	243	3.8
Lipid 0% 2 mm	1.67	247	3.9
Lipid 2% 2 mm	1.68	247	4.1
Lipid 5% 2 mm	1.70	225	4.3
Lipid 10% 2 mm	1.70	231	4.3

despite the spectral distortion caused by water absorption and light scattering. Although the achievable axial resolutions calculated from the spectra were slightly decreased compared with those measured without mixtures, presumably due to the spectral redshift and slight change of the spectral shape, this result indicated that 1.7-μm OCT imaging with an axial resolution of ~4.3 μm in tissue is feasible in deep sites inside turbid scattering tissue, even with 70 volume % of H_2O.

Figure 8 shows the second-order derivative of the phase for the interference signals measured through the mixtures. Compared with the case where a mixture was absent, the second-order derivative strongly depended on the wavelength. This means the dispersion mismatching between the sample and reference arms became notably large due to the chromatic dispersion induced by the mixtures. Because of the large dispersion mismatch, the OCT signals were significantly blurred, as shown in Figs. 5(a) and 5(b). However, the amount of induced dispersion mismatching was almost independent of the lipid concentration. This result indicates that the dispersion mismatching was induced mainly by chromatic dispersion of water, and it is possible to perform deep-tissue imaging with high axial resolution by compensating for the dispersion mismatching in 1.7-μm OCT.

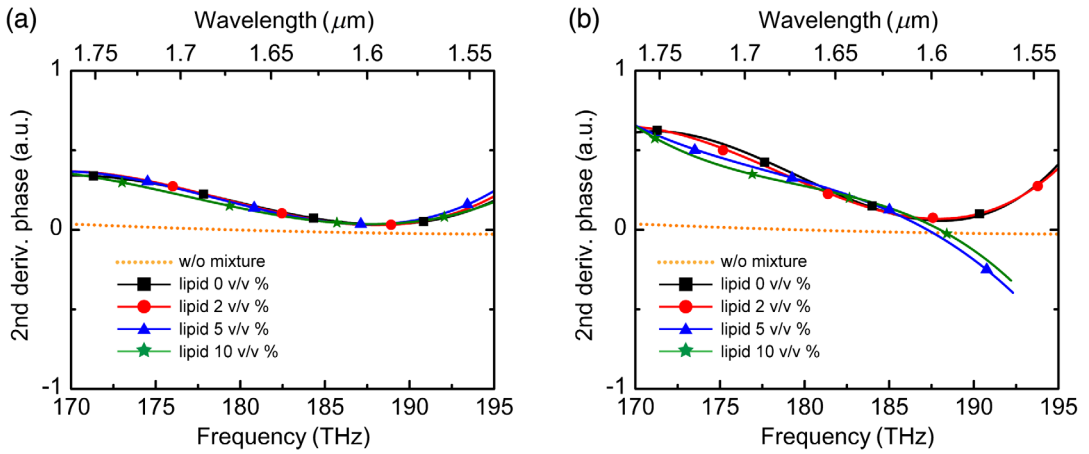

Fig. 8 Second derivative of the phase curve of the interference signals for (a) 1- and (b) 2-mm-thick mixtures. Square, circle, triangle, and star correspond 0, 2, 5, and 10 v/v % lipid concentration, respectively. Note that the number of the actual plotted points are much larger than that of the symbols, and the symbols are displayed only for the purpose to distinguish each line.

3.3 *Dispersion Compensation for High-Axial-Resolution Imaging*

To perform 1.7-μm OCT imaging deep inside samples with high axial resolution, we compensated for the dispersion mismatch using optical glasses (BK7 and fused silica) that have anomalous group velocity dispersion (GVD) in the 1.7-μm wavelength band, as well as water (H_2O).[40] To estimate the glass thickness of BK7 and fused silica required to reduce the dispersion mismatching caused by H_2O as much as possible, we first measured the GVD of H_2O in the wavelength

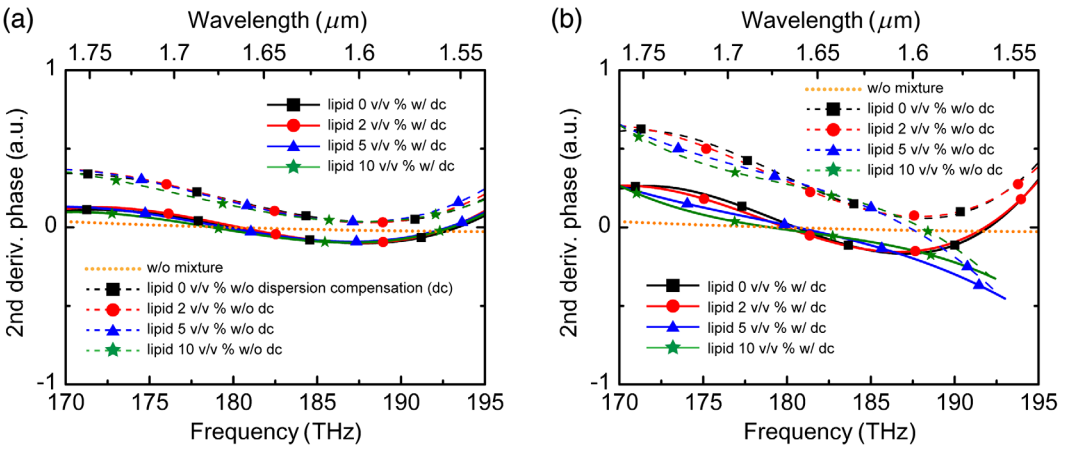

Fig. 9 Second derivative of the phase curve of the interference signals before and after applying dispersion compensation for (a) 1- and (b) 2-mm-thick mixtures. The solid and dashed lines correspond to cases after and before applying dispersion compensation, respectively. The dotted line (orange color) indicates the case without any mixtures. Square, circle, triangle, and star correspond 0, 2, 5, and 10 v/v % lipid concentration, respectively. Note that the number of the actual plotted points are much larger than that of the symbols, and the symbols are displayed only for the purpose to distinguish each line.

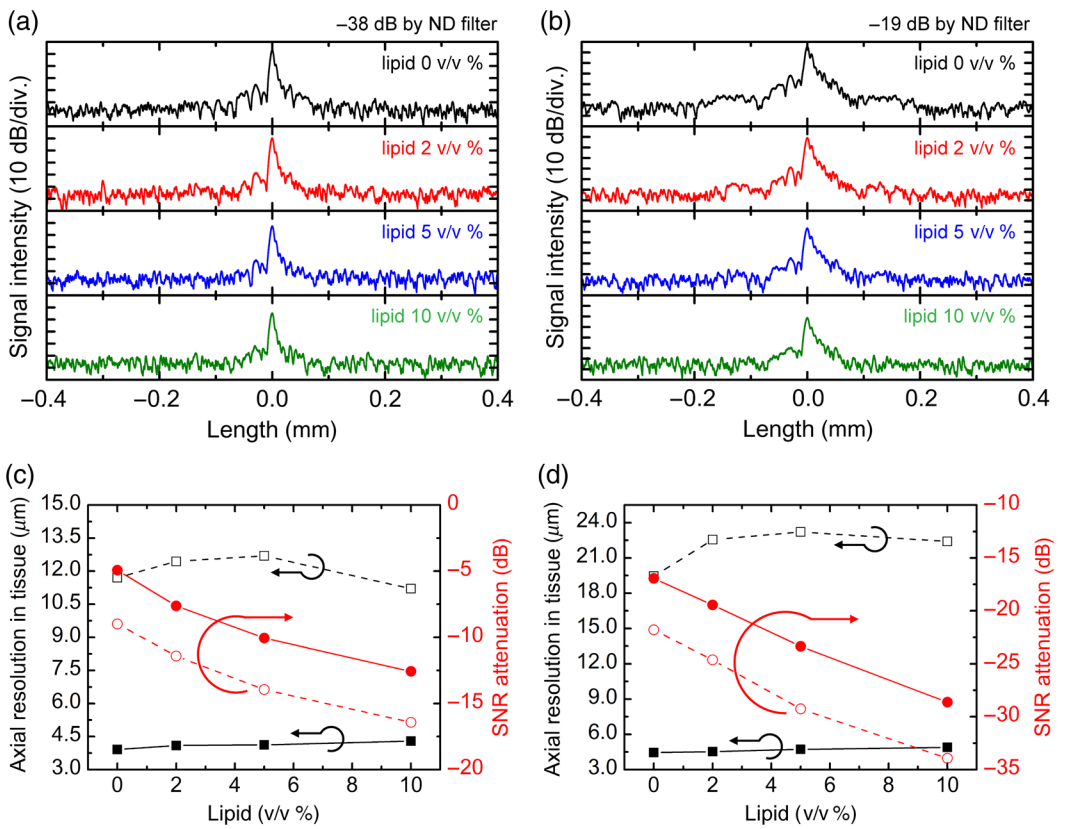

Fig. 10 OCT signals obtained with dispersion compensation for (a) 1- and (b) 2-mm-thick mixtures. Black, red, blue, and green lines correspond to the lipid concentrations of 0%, 2%, 5%, and 10%, respectively. A summary of the axial resolution and SNR attenuation as a function of the lipid concentration is shown in (c) and (d). The solid and dashed lines correspond to cases with and without dispersion compensation, respectively.

band. Based on the result of this measurement, we chose 5-mm-thick BK7 and 2-mm-thick fused silica glass plates to compensate for the dispersion induced by the 1-mm-thick mixture. By placing the glass plates in the reference arm, the second-order derivative of the phase curve became close to zero for all wavelengths [Fig. 9(a)], which means that the dispersion mismatch was almost completely compensated for. For the 2-mm-thick mixture, we compensated for the dispersion mismatch using a 15-mm-thick BK7 glass plate [Fig. 9(b)]. Because BK7 and fused silica glasses have high and flat transmittance characteristics around the 1.7-μm wavelength region, the signal loss and spectral distortion in the reference beam were negligibly small.

Figures 10(a) and 10(b) show the OCT signals obtained with the dispersion compensation. Compared with the OCT signals obtained without the dispersion compensation [Figs. 5(a) and 5(b)], the OCT signals became significantly narrower. In the OCT signals obtained through the 2-mm-thick mixtures, the shapes of the OCT signals became slightly asymmetrical. This is presumably due to the third-order dispersion effect, which was not compensated for by the optical glass plates.[7] The axial resolution and SNR attenuation for the 1- and 2-mm-thick mixtures are summarized in Figs. 10(c) and 10(d), respectively. For both cases, the axial resolution was ~4.3 μm, which is close to the achievable axial resolution determined from the spectral bandwidth (FWHM), spectral shape, and center wavelength (Table 1). Compared with the OCT signal in Fig. 4(a), the OCT signals in Fig. 10(a) have smaller shoulders around the main peak due to the spectral shape being changed. In addition, the SNR was also improved by ~5 dB for all cases by applying the dispersion compensation.

3.4 *Optical Coherence Tomography Imaging of a Biological Sample with Dispersion Compensation*

To demonstrate 1.7-μm high-resolution OCT imaging of biological tissue with the dispersion compensation, we observed a hamster's cheek pouch immersed in phosphate-buffered saline (PBS) because this sample has simple layer structures that are thin enough to easily evaluate the change of the axial resolution in OCT imaging (Fig. 11). The sample was formalin-fixed, meaning that it was dehydrated. Therefore, to mimic a practical situation, we observed the structure through a PBS layer with a thickness of ~1 mm. Figures 11(a) and 11(b) show the obtained OCT images of the sample with and without dispersion compensation, respectively. Each OCT image was formed by averaging 10 OCT images obtained from the same area to improve the SNR. In the OCT image obtained with the dispersion compensation [Fig. 11(a)], thin layered structures in the connective tissue band (Conn) were clearly distinguished. Furthermore, because the SNR was also improved by the dispersion compensation, the muscle layer (Musc) located in the deep part was clearly visualized in Fig. 11(a). On the other hand, they were severely blurred without the dispersion compensation [Fig. 11(b)]. Intensity line profiles of a thin layered structure located in the connective tissue band are shown in Fig. 11(e) for the cases with and without dispersion compensation. From these intensity line profiles, we confirmed that the width (−6 dB from the peak) of the thin layer in the cheek pouch was reduced by a factor of ~1.6 by applying the dispersion compensation. This result is clear evidence that the dispersion compensation allowed us to perform 1.7-μm OCT imaging deep inside tissue with high axial resolution.

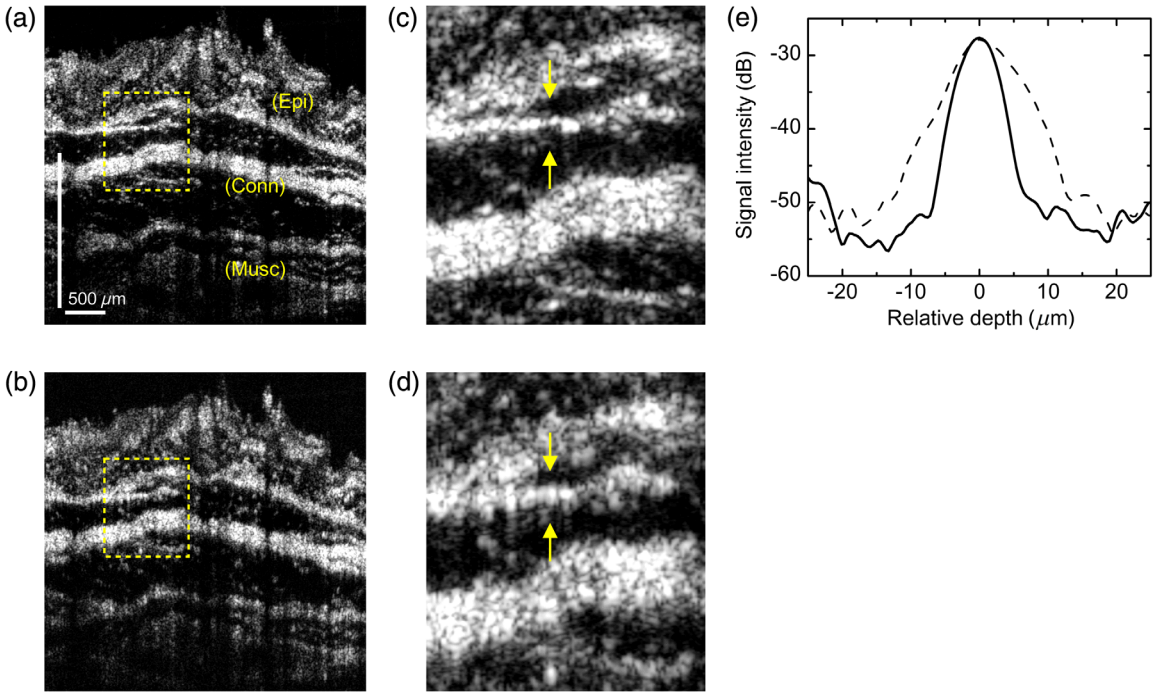

Fig. 11 OCT images of a hamster's cheek pouch obtained (a) with dispersion compensation and (b) without dispersion compensation. (Epi, epidermis layer; Conn, connective tissue layer; and Musc, muscular layer.) (c) and (d) Enlarged images of the areas surrounded by yellow dotted lines in (a) and (b). (e) Line plots of OCT signals of a thin layered structure indicated by yellow arrows in (c) and (d) (solid: with compensation and dashed: without compensation).

4 Discussion and Conclusion

In this work, we examined the impact of light scattering, water absorption, and chromatic dispersion induced by turbid scattering tissue on the axial resolution and SNR in 1.7-μm high-resolution OCT imaging. Our results showed that, in 1.7-μm high-resolution OCT imaging of biological tissue, the axial resolution was decreased mainly due to the dispersion mismatch induced by water in the samples and it was possible to achieve an axial resolution of ~4.3 μm in tissue even in the turbid tissues just by applying dispersion compensation. We also confirmed that the dispersion compensation helped to achieve not only high axial resolution but also improved SNR in deep-tissue OCT imaging.

Our results clearly indicated that the chromatic dispersion induced by water was the main factor to degrade the axial resolution in 1.7-μm high-resolution OCT imaging of the tissue phantom, and the effects of multiple scattering are small enough, as shown in Figs. 5 and 6. As already mentioned previously in this report, the scattering coefficients of this tissue phantom are similar to those of tissues, such as skin and brain. Therefore, our results using the mixture of lipid, H_2O, and D_2O are presumed enough to imitate the case when we observe such tissue specimens (~70 v/v %) with 1.7-μm high-resolution OCT. However, the results would become different for different samples with much higher scattering coefficients even in the 1.7-μm wavelength region or much lower water contents.

For the demonstration of tissue imaging, we used a formalin-fixed hamster's cheek pouch to avoid the structural change during observations. It is known that the formalin-fixation process causes tissue dehydration.[43] It is also reported that the scattering coefficient of samples is also increased by the formalin-fixation process due to protein cross linkage, sample dehydration, and shrinkage. In addition, the absorption coefficients would also increase if intrinsic chromophores in samples are not damaged during the fixation process. Therefore, it is difficult to mimic actual situations in observations of nonfixed samples using only the fixed sample. In our study, to mimic situations as close to actual as possible, the fixed sample was immersed in PBS buffer so that interference signals from the fixed sample were measured through 1-mm-thick layer of PBS solution. Because the main factor to degrade the axial resolution of 1.7-μm OCT in observations of samples with ~70 v/v % H_2O is chromatic dispersion by water, not multiple scattering as shown in Figs. 5 and 6, it is considered that our experiment demonstrated the similar burring of the axial resolution as in the case when we observed 1-mm-depth position of nonfixed samples, especially near the upper surface of the fixed sample.

In this study, to compensate for the dispersion mismatching, we used optical glasses placed in the reference arm. As shown in Figs. 10 and 11, this approach works moderately well. However, as already reported in Refs. 44 and 45, it is difficult to compensate for dispersion mismatching only using optical glasses when second-order dispersion changes complicatedly as a function of wavelength and the effects of higher order dispersion are obvious. This issue can be overcome using numerical compensation methods.[44–48] To demonstrate that

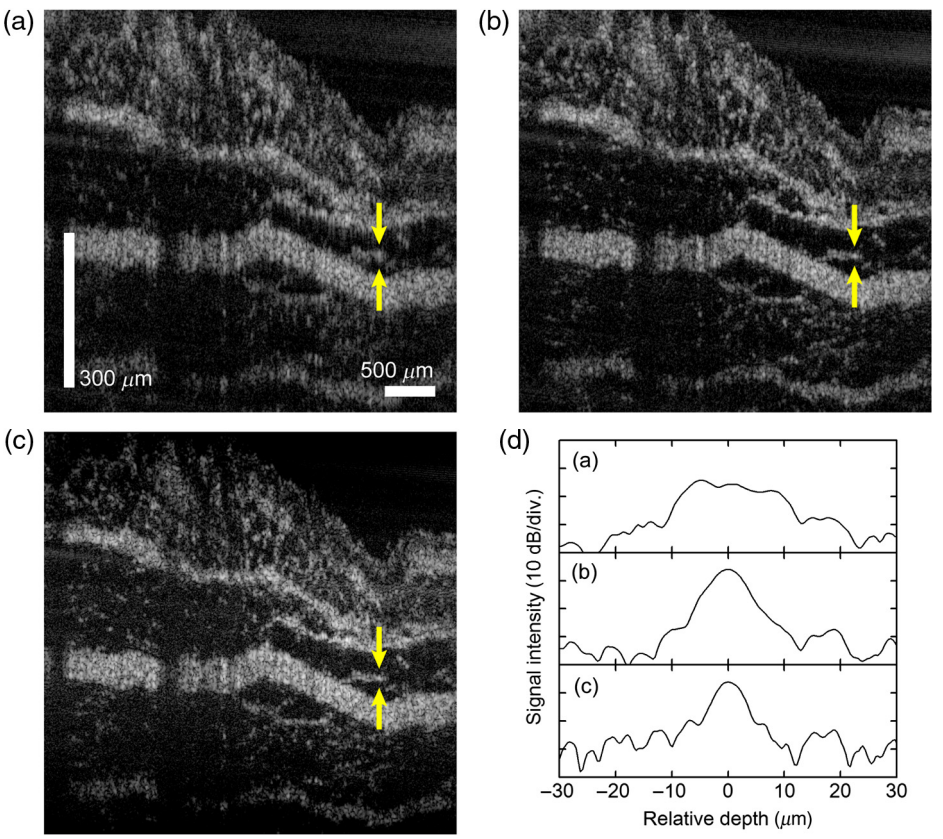

Fig. 12 OCT images of a hamster's cheek pouch obtained (a) before dispersion compensation and (b) after dispersion compensation with optical glass plates placed in the reference arm of the OCT interferometer. (c) OCT image of the sample with applying numerical dispersion compensation to the data (a). (d) Line profile of the thin structure in the sample indicated by yellow arrows.

numerical compensation methods are also useful for 1.7-μm high-resolution OCT, we recorded interference signals from the same sample as that in Fig. 11 (hamster's cheek pouch). In this experiment, we again immersed the sample in a PBS buffer solution so that we observed the sample through a 1-mm-thick layer of PBS solution as in the case of Fig. 11. Figures 12(a)–12(c) are OCT images without dispersion compensation, with dispersion compensation by glass plates (5-mm-thick BK7 and 2-mm-thick fused silica), and with numerical dispersion compensation, respectively. The intensity line profile of the structure indicated with the yellow arrows is shown in Fig. 12(d). Comparing the three intensity line profiles, we confirmed that the numerical approach worked to achieve high axial resolution, which was slightly better than that obtained by glass-based dispersion compensation. This time, we took into account second- and third-order dispersion in this numerical approach. The axial resolution might be improved more by taking into account higher order dispersions and then optimizing parameters for this numerical calculation.

We also noted that the axial resolution of the 1.7-μm OCT in deep-tissue imaging would be limited to ~4 μm in tissue specimens with ~70 v/v % H_2O, where the refractive index is assumed to be 1.38. Although an axial resolution of ~1 μm can be achieved with a 900-nm spectral band (FWHM) light source for the case where the scattering and water absorption are negligible, the spectral width would be narrowed to ~230 nm, which corresponds almost to the spectral width of the local minimum of the water absorption located around the 1.7-μm wavelength window due to the strong water absorption peaks at 1.45 and 1.9 μm and a large scattering coefficient in the shorter-wavelength region.

As with typical OCT systems, the low-numerical aperture (NA) lens was used as an objective lens to obtain a long imaging depth range of around 2 mm. Therefore, the lateral resolution of our 1.7-μm OCT system was ~23 μm, which was not as high as the axial resolution. Considering the beam diameter (3 mm) and the focal length of the focusing achromatic lens (30 mm), this lateral resolution was close to the diffraction limit of the lateral resolution of ~21 μm. Although we used the light source with ~500 nm spectral bandwidth, this fact indicated that the laser beam was well focused and the size of the laser focus was close to the diffraction limit. Although the imaging depth range is reduced, it would be possible to improve both the lateral and axial resolution using OCM with a high-NA objective lens.[12,20] For example, if we used an objective lens with an NA of 1.0, a lateral resolution of ~0.85 μm and an axial resolution of ~2.3 μm would be achieved using only a confocal gate. In OCM, the axial resolution is determined by the combination of coherent and confocal gates. Therefore, even if spectral narrowing occurs or we use a light source with a narrower spectral bandwidth, we could achieve improved axial resolution in 1.7-μm OCM with a high-NA objective lens.

In this study, we used the OCT system with time-domain interferometry, and the sensitivity of the OCT system was ~93 dB when the incident laser power was 3 mW, which is below the American National Standards Institute damage threshold for skin tissue (9.6 mW for the 1.5- to 1.8-μm wavelength region). This detection sensitivity could be improved if we employ a Fourier-domain (FD) scheme, including a spectral-domain (SD) and swept-source domain scheme, for 1.7-μm OCT.[49] Because the acquisition speed of OCT images in FD-OCT is typically tens times faster than TD-OCT, the higher SNR can be achieved in FD-OCT by averaging OCT images and reducing the noise fluctuation still with higher acquisition speed. In our group, we have recently developed 1.7-μm full-range SD-OCT with the same ultrabroadband light source as what we used in this study and realized the penetration depth of ~1.7 mm in observations of a formalin-fixed mouse brain. If we apply both the glass-based and numerical dispersion compensations shown in this study to the 1.7-μm full-range SD-OCT, it would become possible to improve the axial resolution, the SNR, and the penetration depth.

In this paper, we reported that 1.7-μm high-resolution OCT imaging is feasible even in deep sites inside biological tissue just by compensating for the dispersion mismatching between the sample and reference arms. Although the spectral shape of the interference signals was distorted, we confirmed that, with dispersion compensation, the axial resolution was improved to ~4.3 μm in tissue and the SNR was improved.

Disclosures

The authors have no relevant financial interests in this paper and no potential conflicts of interest to disclose.

References

1. D. Huang et al., "Optical coherence tomography," *Science* **254**, 1178–1181 (1991).
2. W. Drexler et al., "Optical coherence tomography today: speed, contrast, and multimodality," *J. Biomed. Opt.* **19**(7), 071412 (2014).
3. W. Drexler et al., "In vivo ultrahigh-resolution optical coherence tomography," *Opt. Lett.* **24**, 1221–1223 (1999).
4. I. Hartl et al., "Ultrahigh-resolution optical coherence tomography using continuum generation in an air-silica microstructure optical fiber," *Opt. Lett.* **26**, 608–610 (2001).
5. B. Povazay et al., "Submicrometer axial resolution optical coherence tomography," *Opt. Lett.* **27**, 1800–1802 (2002).
6. J. G. Fujimoto, "Optical coherence tomography for ultrahigh resolution in vivo imaging," *Nat. Biotechnol.* **21**, 1361–1367 (2003).
7. W. Drexler and J. G. Fujimoto, Eds., *Optical Coherence Tomography*, Springer International Publishing, Switzerland (2015).
8. M. Adhi et al., "Optical coherence tomography—current and future applications," *Curr. Opin. Ophthalmol.* **24**(3), 213–221 (2013).
9. E. Sattler et al., "Optical coherence tomography in dermatology," *J. Biomed. Opt.* **18**(6), 061224 (2013).
10. E. Osiac et al., "Optical coherence tomography as a promising imaging tool for brain investigations," *Rom. J. Morphol. Embryol.* **55**, 507–512 (2014).
11. A. Alex et al., "Multispectral in vivo three-dimensional optical coherence tomography of human skin," *J. Biomed. Opt.* **15**, 026025 (2010).
12. V. J. Srinivasan et al., "Optical coherence microscopy for deep tissue imaging of the cerebral cortex with intrinsic contrast," *Opt. Express* **20**, 2220–2239 (2012).
13. L. A. Sordillo et al., "Deep optical imaging of tissue using the second and third near-infrared spectral windows," *J. Biomed. Opt.* **19**(5), 056004 (2014).
14. N. G. Horton et al., "In vivo three-photon microscopy of subcortical structures within an intact mouse brain," *Nat. Photonics* **7**, 205–209 (2013).
15. S. Diao et al., "Fluorescence imaging in vivo at wavelengths beyond 1500 nm," *Angew. Chem.* **127**, 14971–14975 (2015).
16. V. M. Kodach et al., "Quantitative comparison of the OCT imaging depth at 1300 nm and 1600 nm," *Biomed. Opt. Express* **1**(1), 176–185 (2010).
17. U. Sharma et al., "Long-wavelength optical coherence tomography at 1.7 μm for enhanced imaging depth," *Opt. Express* **16**(24), 19712–19723 (2008).
18. S. Ishida et al., "Ultrahigh-resolution optical coherence tomography in 1.7 μm region with fiber laser supercontinuum in low-water-absorption samples," *Appl. Phys. Express* **4**, 052501 (2011).

19. S. Ishida et al., "Quantitative comparison of contrast and imaging depth of ultrahigh-resolution optical coherence tomography images in 800–1700 nm wavelength region," *Biomed. Opt. Express* **3**(2), 282–294 (2012).
20. M. Yamanaka et al., "Optical coherence microscopy in 1700 nm spectral band for high-resolution label-free deep-tissue imaging," *Sci. Rep.* **6**, 31715 (2016).
21. H. Kawagoe et al., "Full-range ultrahigh-resolution spectral-domain optical coherence tomography in 1.7 μm wavelength region for deep-penetration and high-resolution imaging of turbid tissues," *Appl. Phys. Express* **9**, 127002 (2016).
22. M. Tanaka et al., "1.7 μm spectroscopic spectral-domain optical coherence tomography for imaging lipid distribution within blood vessel," *Opt. Express* **23**(5), 6645–6655 (2015).
23. S. P. Chong et al., "Noninvasive, in vivo imaging of subcortical mouse brain regions with 1.7 μm optical coherence tomography," *Opt. Lett.* **40**(21), 4911–4914 (2015).
24. C. K. Hitzenberger et al., "Dispersion effects in partial coherence interferometry: implications for intraocular ranging," *J. Biomed. Opt.* **4**(1), 144–151 (1999).
25. A. F. Fercher et al., "Dispersion compensation for optical coherence tomography depth-scan signals by a numerical technique," *Opt. Commun.* **204**, 67–74 (2002).
26. T. R. Hillman and D. D. Sampson, "The effect of water dispersion and absorption on axial resolution in ultrahigh-resolution optical coherence tomography," *Opt. Express* **13**(6), 1860–1874 (2005).
27. S. Hariri et al., "Limiting factors to the OCT axial resolution for in-vivo imaging of human and rodent retina in the 1060 nm wavelength range," *Opt. Express* **17**(26), 24304–24316 (2009).
28. S. Marschall, C. Pedersen, and P. E. Andersen, "Investigation of the impact of water absorption on retinal OCT imaging in the 1060 nm range," *Biomed. Opt. Express* **3**(7), 1620–1631 (2012).
29. S. T. Flock et al., "Optical properties of intralipid: a phantom medium for light propagation studies," *Lasers Surg. Med.* **12**, 510–519 (1992).
30. B. W. Pogue and M. S. Patterson, "Review of tissue simulating phantoms for optical spectroscopy, imaging and dosimetry," *J. Biomed. Opt.* **11**(4), 041102 (2006).
31. K. Naganuma, K. Mogi, and H. Yamada, "Group-delay measurement using the Fourier transform of an interferometric cross correlation generated by white light," *Opt. Lett.* **15**(7), 393–395 (1990).
32. T. Fuji et al., "Linear propagation of light investigated with a white-light Michelson interferometer," *J. Opt. Soc. Am. B* **14**(5), 1074–1078 (1997).
33. T. Hellmuth and M. Welle, "Simultaneous measurement of dispersion, spectrum, and distance with a Fourier transformation spectrometer," *J. Biomed. Opt.* **3**(1), 7–11 (1998).
34. L. Shi et al., "Transmission in near-infrared optical windows for deep brain imaging," *J. Biophotonics* **9**(1–2), 38–43 (2016).
35. H. Neeb et al., "Fast quantitative mapping of absolute water content with full brain coverage," *NeuroImage* **42**, 1094–1109 (2008).
36. H. Arimoto and M. Egawa, "Imaging wavelength and light penetration depth for water content distribution measurement of skin," *Skin Res. Technol.* **21**, 94–100 (2015).
37. Y. Wang et al., "Measurement of absorption spectrum of deuterium oxide (D_2O) and its application to signal enhancement in multiphoton microscopy at the 1700-nm window," *Appl. Phys. Lett.* **108**, 021112 (2016).
38. L. Kou, D. Labrie, and P. Chylek, "Refractive indices of water and ice in the 0.65- to 2.5-μm spectral range," *Appl. Opt.* **32**(19), 3531–3540 (1993).
39. J. G. Bayly, V. B. Kartha, and W. H. Stevens, "The absorption spectra of liquid phase H_2O, HDO and D_2O from 0.7 μm to 10 μm," *Infrared Phys.* **3**, 211–222 (1963).
40. N. G. Horton and C. Xu, "Dispersion compensation in three-photon fluorescence microscopy at 1,700 nm," *Biomed. Opt. Express* **6**(4), 1392–1397 (2015).
41. G. B. Altshuler, R. R. Anderson, and D. Manstein, "Method and apparatus for the selective targeting of lipid-rich tissue," U.S. Patent No. 6,605,080 B1.
42. R. K. Wang, "Signal degradation by multiple scattering in optical coherence tomography of dense tissue: a Monte Carlo study towards optical clearing of biotissues," *Phys. Med. Biol.* **47**, 2281–2299 (2002).
43. A. Pitzschke et al., "Optical properties of rabbit brain in the red and near-infrared: changes observed under in vivo, postmortem, frozen, and formalin-fixated conditions," *J. Biomed. Opt.* **20**(2), 025006 (2015).
44. A. F. Fercher et al., "Numerical dispersion compensation for partial coherence interferometry and optical coherence tomography," *Opt. Express* **9**(12), 610–615 (2001).
45. M. Wojtkowski et al., "Ultrahigh-resolution, high-speed, Fourier domain optical coherence tomography and methods for dispersion compensation," *Opt. Express* **12**(11), 2404–2422 (2004).
46. W. Choi et al., "Extracting and compensating dispersion mismatch in ultrahigh-resolution Fourier domain OCT imaging of the retina," *Opt. Express* **20**(23), 25357–25368 (2012).
47. N. Lippok et al., "Dispersion compensation in Fourier domain optical coherence tomography using the fractional Fourier transform," *Opt. Express* **20**(21), 23398–23413 (2012).
48. Y. Yasuno et al., "In vivo high-contrast imaging of deep posterior eye by 1-μm swept source optical coherence tomography and scattering optical coherence angiography," *Opt. Express* **15**(10), 6121–6139 (2007).
49. R. Leitgeb, C. K. Hitzenberger, and A. F. Fercher, "Performance of Fourier domain vs. time domain optical coherence tomography," *Opt. Express* **11**(8), 889–894 (2003).

Biographies for the authors are not available.